ResearchGate

See discussions, stats, and author profiles for this publication at: https://www.researchgate.net/publication/335145174

Oxygen-assisted synthesis of hBN films for resistive random access memories

Article *in* Applied Physics Letters · August 2019

DOI: 10.1063/1.5100495

CITATIONS
0

READS
75

5 authors, including:

Weiyi Lin
Xiamen University

16 PUBLICATIONS 99 CITATIONS

SEE PROFILE

All content following this page was uploaded by Weiyi Lin on 20 October 2019.

The user has requested enhancement of the downloaded file.

Applied Physics Letters

Oxygen-assisted synthesis of hBN films for resistive random access memories

Cite as: Appl. Phys. Lett. **115**, 073101 (2019); https://doi.org/10.1063/1.5100495
Submitted: 17 April 2019 . Accepted: 28 July 2019 . Published Online: 12 August 2019

Weiyi Lin, Pingping Zhuang, Deji Akinwande, Xue-Ao Zhang, and Weiwei Cai

View Online

Export Citation

CrossMark

AIP Publishing

© 2019 Author(s).

Applied Physics Letters ARTICLE scitation.org/journal/apl

Oxygen-assisted synthesis of hBN films for resistive random access memories

Cite as: Appl. Phys. Lett. **115**, 073101 (2019); doi: 10.1063/1.5100495
Submitted: 17 April 2019 · Accepted: 28 July 2019 ·
Published Online: 12 August 2019

View Online

Export Citation

CrossMark

Weiyi Lin,[1,2] Pingping Zhuang,[1,2] Deji Akinwande,[2] Xue-Ao Zhang,[1] and Weiwei Cai[1,a)]

AFFILIATIONS

[1]Department of Physics, Key Laboratory of Low Dimensional Condensed Matter Physics, Jiujiang Research Institute, Xiamen University, Xiamen 361005, China
[2]Department of Electrical and Computer Engineering, The University of Texas at Austin, Austin, Texas 78757, USA

[a)]Author to whom correspondence should be addressed: wwcai@xmu.edu.cn

ABSTRACT

In this letter, we report an oxygen-assisted chemical vapor deposition method to synthesize uniform large-area high-quality multilayer hexagonal boron nitride (hBN) films (denoted by O-hBN). Nonvolatile bipolar resistive switching (RS) of resistive random access memories (RRAMs) based on O-hBN films is presented. These RRAMs exhibit enhanced RS performance with lower cycle-to-cycle variability, lower set voltage, and higher current on/off ratio. The enhancement is benefited from the clean and smooth surface of O-hBN films and the reduction of grain boundaries which serve as an energetically favored path for ion migration. This scalable approach to synthesize hBN films could facilitate practical applications of hBN-based RRAMs.

Published under license by AIP Publishing. https://doi.org/10.1063/1.5100495

Resistive random access memory (RRAM) with metal-insulator-metal (MIM) stacks is a promising technology for digital information storage and calculation.[1] To date, state-of-the-art RRAMs use transition metal oxides (TMOs), which are sandwiched by metal electrodes and serve as resistive switching (RS) media.[2–7] By tuning applied electrical bias, the resistance of TMO can be set to low resistive states (LRS) and be reset to high resistive states (HRS), which correspond to ones and zeros of the binary code, respectively.[8] Compared with TMO materials, two-dimensional (2D) hexagonal boron nitride (hBN) with high flexibility,[9] transparency,[10] and thermal conductivity[11] is expected to provide additional capabilities to RRAMs. Recently, the nonvolatile RS of hBN-based RRAMs has been demonstrated by the pioneering experimental study.[12] The achievement of RS operations is determined by reversible conductive filaments (CFs) that are composed of metal ions from electrodes.[13–15] Aligned grain boundaries (GBs) of hBN play a crucial role because the penetration of metal ions into hBN layers along boron-vacancy-rich GBs is in an energetically favored path.[16] Therefore, the optimized synthesis of hBN films to enhance RS performance is a key requirement for hBN-based RRAM technology. In this letter, we report an oxygen-assisted chemical vapor deposition (CVD) of multilayer hBN films (O-hBN). Compared with RRAMs based on hBN films that are synthesized without an oxygen supply, devices using O-hBN exhibit nonvolatile bipolar RS behavior with lower cycle-to-cycle variability, lower set voltage (V_{set}), and higher resistance in HRS.

Copper foils used to deposit hBN are pretreated by electrochemical polishing to obtain a smooth metal surface.[17,18] Then, hBN films are synthesized on these foils by the CVD method using ammonia-borane powders as the precursor. The integrated CVD process consists of three parts: (i) injecting a mixture gas flow of 20-mTorr air (controlled by a needle valve) and 10-sccm hydrogen (determined by a mass flow controller) into the tube, and simultaneously heating the furnace up to 1030 °C to anneal the copper foil; (ii) heating the AB powder up to 80 °C by a water bath and maintaining 10 min to deposit continuous hBN films; (iii) cooling the furnace tube rapidly after removing the water bath. Figure 1(a) shows a scanning electron microscopy (SEM) image of O-hBN films on the copper foil. We can clearly discern boundaries of copper grains and few white nanoparticles that are adsorbed on this clean O-hBN film with wrinkles. By contrast, the hBN obtained without oxygen assistance presents a nonuniform appearance with a number of impurities [Fig. 1(b)]. After being transferred onto SiO_2/Si substrates, these films are characterized by atomic force microscopy (AFM), showing the thickness of O-hBN [Fig. 1(c)] and hBN films [Fig. 1(d)]. Note that the morphology and quality of both hBN and O-hBN films can vary sample-to-sample even using the same synthesizing recipe. Statistically, O-hBN films are of higher quality, e.g., uniform cleaning surfaces, larger size, and higher orientation consistency of triangle domains that join to form continuous films as presented in our previous study.[17]

Published under license by AIP Publishing

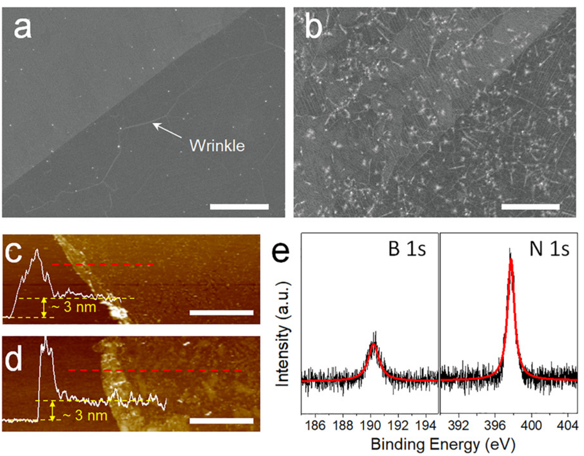

FIG. 1. Scanning electron microscopy (SEM) images of both (a) O-hBN and (b) hBN films both on copper foils. Atomic force microscopy (AFM) images and height profiles of transferred (c) O-hBN and (d) hBN films both on SiO_2/Si substrates. (e) X-ray photoelectron spectroscopy (XPS) spectra of B-1s and N-1s core levels of transferred O-hBN films. Spectral data are fitted by symmetric Lorentzians (red curves). Scale bar = 5 μm.

X-ray photoelectron spectroscopy (XPS) measurements are used to characterize the elemental stoichiometry and bonding configuration of the transferred O-hBN film. Figure 1(e) shows both core-level peaks at 190.2 eV (B 1s) and 397.7 eV (N 1s) with a 1:1.01 B/N atomic ratio. These values are in good agreement with previous reports on CVD-grown hBN.[19] Moreover, both peaks are in symmetric shapes that can be perfectly fitted by single Lorentzians. This spectral feature indicates that each B (N) atom is bound with atoms of one kind of elements, that is, the configuration for B and N atoms is the B-N bond. Therefore, the oxygen injected during CVD processes does not lead to substituted doping to the lattice atoms of the synthesized O-hBN film.

To investigate the RS performance, we fabricate Ti/hBN/Au MIM devices based on these hBN films on a SiO_2/Si wafer using standard UV lithography and e-beam evaporation processes [supplementary material; Figs. 2(a) and 2(b)]. As shown in Fig. 2(c), the Raman spectrum obtained at the location closed to a MIM crossbar stack shows the appearance of two peaks located at 1369 cm^{-1} (E_{2g} phonon of hBN) and 1450 cm^{-1} (third-order transverse optic phonon of silicon), demonstrating the existence of a high-quality O-hBN film.[20,21]

These hBN MIM devices are characterized on a Cascade probe station with an Agilent 4156 semiconductor parameter analyzer. By applying bias to TE, these devices exhibit nonvolatile bipolar RS, where the positive bias set hBN to LRS and negative bias the vice versa. Due to the migration of boron ions under the electric field, Ti ions are capable of diffusing into hBN along the aligned grain boundaries.[11,15] These charged Ti ions can be reduced to neutral atoms by contacting with grounded BE and form CFs that connect both electrodes eventually, thus setting the resistive state of hBN from HRS to LRS. Under negative bias, the CFs can be ruptured by field-induced ion diffusion and/or thermal-assisted filament melting, resetting the device to HRS. To validate the CF-related switching mechanism, we plot the positive bias sweep (set operation) of I-V characteristics on a double logarithmic scale for hBN [Fig. 3(a)] and O-hBN devices [Fig. 3(b)]. Both I-V curves in the LRS exhibit a linearly Ohmic behavior with a slope of ~1, implying the formation of CFs in hBN films during the set process. As the voltage gradually increases, however, I-V curves of the

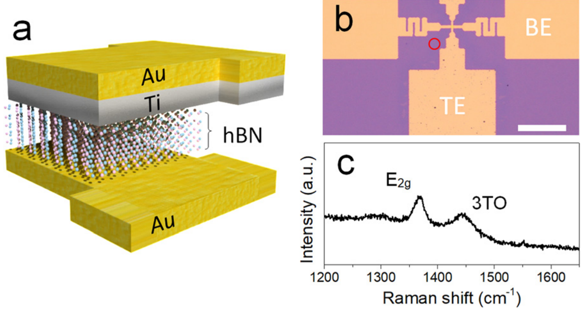

FIG. 2. (a) and (b) Schematic and optical image of hBN MIM structures. The BE and TE denote bottom and top electrodes, respectively. Scale bar = 50 μm. (c) Raman spectrum taken at the location that is marked by a red circle in (b). Peaks located at 1369 cm^{-1} and 1450 cm^{-1} indicate the E_{2g} phonon mode of hBN and third-order transverse optic phonon mode (3TO) of silicon. The incident photon energy is 2.33 eV.

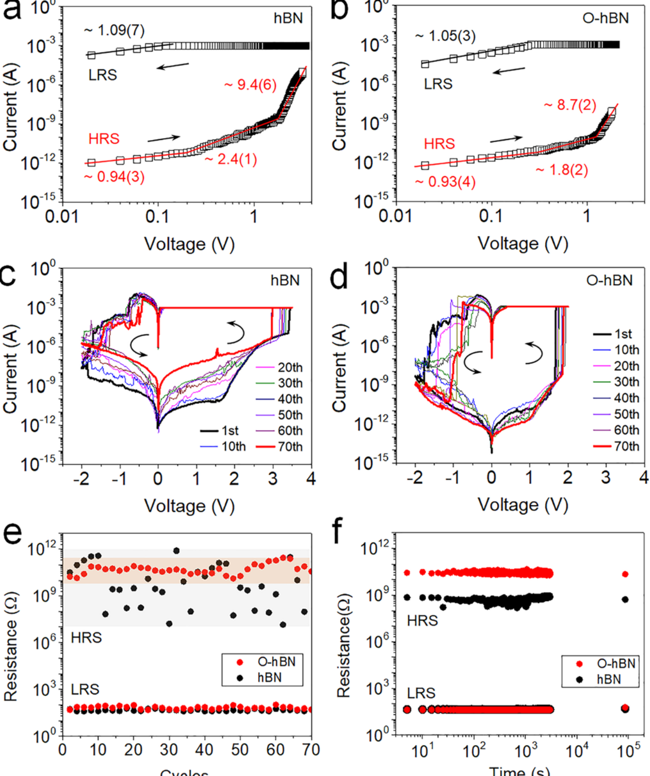

FIG. 3. The linear fitting of the I-V curve of (a) hBN and (b) O-hBN RRAMs on a double logarithmic scale. Numerical values are the corresponding slopes for each portion. (c) and (d) Nonvolatile bipolar RS of hBN and O-hBN RRAMs. (e) The endurance of hBN and O-hBN RRAMs with manual DC switching cycles. (f) The resistive-state retention time of hBN and O-hBN RRAMs over 24 h at ambient conditions. The resistance is determined by the current read at the bias of 50 mV.

Published under license by AIP Publishing

HRS sequentially show the Ohmic region ($I \propto V$), the Child's law region ($I \propto V^2$), and the steep current increase region ($I \propto V^\alpha$, $\alpha > 2$), which is in good agreement with the space charge limited conduction (SCLC) mechanism.[21] Since the initial state (HRS) reflects the intrinsic conductive properties of hBN films, the different conductive behavior between HRS and LRS indicates that the charge transport in LRS is a localized behavior that is consistent with the CF-related mechanism.

Figures 3(c) and 3(d) show typical $I - V$ curves collected in hBN and O-hBN RRAMs. Compared with the hBN MIM device, the O-hBN device exhibits lower set voltages (V_{set}) and higher current on/off ratios (I_{on}/I_{off}). Moreover, the cycle-to-cycle variability of O-hBN RRAMs is significantly lower than that of hBN RRAMs [Fig. 3(e)]. The capability of resistance-state retention of both HRS and LRS under ambient conditions is also demonstrated, showing the nonvolatile RS characteristics [Fig. 3(f)]. Generally, the reduction of hBN GBs can lead to an increase in V_{set}. As an extreme case, exfoliated hBN films without GBs are ideal 2D dielectric layers that will not exhibit the RS behavior.[22] Compared with the V_{set} of hBN RRAM, the lower value of O-hBN RRAM may originate from the reduced surface roughness instead of the decrease in GBs. The roughness reduction of the O-hBN film can be attributed to the high crystallization and faster growth rate boosted by oxygen. Additionally, the decrease in GBs naturally reduces the number of conductive filaments, thus resulting in a lower value of current in HRS. For experimental data present in this letter, the current limitation in the set process is fixed to 1 mA. In this case, the I_{on}/I_{off} reaches a value up to 10^8. Considering the fact that decreasing the current limitation appropriately can enhance the endurance of RS operations and reduce the V_{reset}, I_{on}/I_{off} is not a strict technology requirement. Despite a device-to-device variability, compared with RRAMs based on the hBN film, O-hBN MIM devices generally exhibit lower V_{set} under fixed current limitation and lower current in HRS. In addition to DC characterization, voltage pulses are applied to these Ti/O-hBN/Au RRAMs, showing a 5 μs set switching speed (supplementary material).

In conclusion, high-quality multilayer hBN are synthesized by the CVD method with the aid of oxygen. The RRAMs based on these O-hBN films show enhanced RS performance, i.e., lower cycle-to-cycle variability, lower V_{set}, and higher electrical resistance of HRS. This scalable synthesizing approach can be a promising method for facilitating the mass production of hBN-based RRAMs with high RS performance in practice. For the real-world applications, challenges including the device stability and switching performance still remain.

See the supplementary material for (S1) fabrication of hBN-based MIM devices and (S2) pulse operation of Ti/O-hBN/Au RRAMs.

This work was supported by the National Natural Science Foundation of China (Grant Nos. 11335006 and 11874423) and Fok Ying Tung Education Foundation. We acknowledge the use of Texas Nanofabrication Facilities supported by the NSF NNCI Award No. 1542159. D. Akinwande acknowledges the support of the PECASE award from the Army Research Office. We also acknowledge the China Scholarship Council (CSC) scholarship under the State Scholarship Fund.

REFERENCES

[1] I. Valov, Chemelectrochem **1**(1), 26–36 (2014).
[2] H. S. P. Wong, H. Y. Lee, S. M. Yu, Y. S. Chen, Y. Wu, P. S. Chen, B. Lee, F. T. Chen, and M. J. Tsai, Proc. IEEE **100**(6), 1951–1970 (2012).
[3] W. A. Hubbard, A. Kerelsky, G. Jasmin, E. R. White, J. Lodico, M. Mecklenburg, and B. C. Regan, Nano Lett. **15**(6), 3983–3987 (2015).
[4] G. Bersuker, D. C. Gilmer, D. Veksler, P. Kirsch, L. Vandelli, A. Padovani, L. Larcher, K. McKenna, A. Shluger, V. Iglesias, M. Porti, and M. Nafria, J. Appl. Phys. **110**(12), 124518 (2011).
[5] I. G. Baek, M. S. Lee, S. Seo, M. J. Lee, D. H. Seo, D. S. Suh, J. C. Park, S. O. Park, H. S. Kim, I. K. Yoo, U. I. Chung, and J. T. Moon, in IEEE International Electron Devices Meeting Technical Digest (2004), pp. 587–590.
[6] Z. Wei, Y. Kanzawa, K. Arita, Y. Katoh, K. Kawai, S. Muraoka, S. Mitani, S. Fujii, K. Katayama, M. Iijima, T. Mikawa, T. Ninomiya, R. Miyanaga, Y. Kawashima, K. Tsuji, A. Himeno, T. Okada, R. Azuma, K. Shimakawa, H. Sugaya, I. Takagi, R. Yasuhara, K. Horiba, H. Kumigashira, and M. Oshima, in IEEE International Electron Devices Meeting Technical Digest (2008), pp. 1–4.
[7] Y. Sharma, S. P. Pavunny, E. Fachini, J. F. Scott, and R. S. Katiyar, J. Appl. Phys. **118**(9), 094506 (2015).
[8] M. Lanza, Materials **7**(3), 2155–2182 (2014).
[9] N. Petrone, T. Cheri, I. Meric, L. Wang, K. L. Shepard, and J. Hone, ACS Nano **9**(9), 8953–8959 (2015).
[10] K. Watanabe, T. Taniguchi, and H. Kanda, Nat. Mater. **3**(6), 404–409 (2004).
[11] I. Jo, M. T. Pettes, J. Kim, K. Watanabe, T. Taniguchi, Z. Yao, and L. Shi, Nano Lett. **13**(2), 550–554 (2013).
[12] F. M. Puglisi, L. Larcher, C. Pan, N. Xiao, Y. Shi, F. Hui, and M. Lanza, in Proceedings of the International Electron Devices Meeting, 2016, pp. 874–877.
[13] Y. Shi, C. Pan, V. Chen, N. Raghavan, K. L. Pey, F. M. Puglisi, E. Pop, H. S. P. Wong, and M. Lanza, in IEEE International Electron Devices Meeting (IEDM), 2017, pp. 119–122.
[14] Y. Y. Shi, X. H. Liang, B. Yuan, V. Chen, H. T. Li, F. Hui, Z. C. W. Yu, F. Yuan, E. Pop, H. S. P. Wong, and M. Lanza, Nat. Electron. **1**(8), 458–465 (2018).
[15] F. Hui, M. A. Villena, W. J. Fang, A. Y. Lu, J. Kong, Y. Y. Shi, X. Jing, K. C. Zhu, and M. Lanza, 2D Mater. **5**(3), 031011 (2018).
[16] C. B. Pan, Y. F. Ji, N. Xiao, F. Hui, K. C. Tang, Y. Z. Guo, X. M. Xie, F. M. Puglisi, L. Larcher, E. Miranda, L. L. Jiang, Y. Y. Shi, I. Valov, P. C. McIntyre, R. Waser, and M. Lanza, Adv. Funct. Mater. **27**(10), 1604811 (2017).
[17] P. P. Zhuang, W. Y. Lin, B. B. Xu, and W. W. Cai, Appl. Phys. Lett. **111**(20), 203103 (2017).
[18] K. Sridhara, B. N. Feigelson, J. A. Wollmershauser, J. K. Hite, A. Nath, S. C. Hernandez, M. S. Fuhrer, and D. K. Gaskill, Cryst. Growth Des. **17**(4), 1669–1678 (2017).
[19] L. Song, L. J. Ci, H. Lu, P. B. Sorokin, C. H. Jin, J. Ni, A. G. Kvashnin, D. G. Kvashnin, J. Lou, B. I. Yakobson, and P. M. Ajayan, Nano Lett. **10**(8), 3209–3215 (2010).
[20] Q. R. Cai, D. Scullion, A. Falin, K. Watanabe, T. Taniguchi, Y. Chen, E. J. G. Santos, and L. H. Li, Nanoscale **9**(9), 3059–3067 (2017).
[21] G. Y. Lu, T. R. Wu, Q. H. Yuan, H. S. Wang, H. M. Wang, F. Ding, X. M. Xie, and M. H. Jiang, Nat. Commun. **6**, 6160 (2015).
[22] Y. Hattori, T. Taniguchi, K. Watanabe, and K. Nagashio, ACS Nano **9**(1), 916–921 (2015).

Published under license by AIP Publishing

View publication stats